Analyst

Accepted Manuscript

ROYAL SOCIETY OF CHEMISTRY

www.rsc.org/analyst

Embedded ceria nanoparticle in gel improves electrophoretic separation: a preliminary demonstration

Mohammad Zarei,[a] Hossein Ahmadzadeh,[a,*] and Elaheh K. Goharshadi [a,b]

Mohammad Zarei: [a] *Department of Chemistry, Ferdowsi University of Mashhad Mashhad 91779, Iran.*

Hossein Ahmadzadeh: [a] *Department of Chemistry, Ferdowsi University of Mashhad Mashhad 91779, Iran*

Elaheh K. Goharshadi: [a] *Department of Chemistry and* [b] *Center of Nano Research Ferdowsi University of Mashhad, Mashhad 91779, Iran.*

■ AUTHOR INFORMATION

Corresponding Author

h.ahmadzadeh@um.ac.ir

Abstract

Slab gel electrophoresis is still the gold standard method for the separation of biomolecules such as proteins and DNA with advantages such as simplicity, affordability, and high throughput; but it suffers from inadequate separation speed and resolution. Single capillary gel electrophoresis, on the other hand, offers faster separation time and improved resolution at the expense of higher cost and loss of high throughput capability. The high surface-to volume ratio of the capillary cause improved heat dissipation leading to a reduced Joule heating and a higher resolution. Here, we show, for the first time, the use of dispersed ceria nanoparticles (NPs) to improve the resolution and speed of protein separation in slab gel electrophoresis. We measured the rheological parameters of separation medium in order to find a meaningful relation between viscosity changes, Joule heating, and band broadening. The results showed that ceria NPs decrease the viscosity of polyacrylamide gel. By loading 0.03 % (w/v) ceria NPs into polyacrylamide gel at 25 $^{\circ}$C, the viscosity decreased 22 % and thermal conductivity increased 81 %, which resulted in 35 % reduction in Joule heating and 47 % increase in resolution. This work is a cross disciplinary of theoretical physical chemistry for thermal conductivity and rheological measurements of ceria NPs and application in slab gel electrophoresis. We report here, for the first time, that embedded NPs in PA gel could potentially interface high throughput capability of slab gel electrophoresis with high separation speed of single capillary electrophoresis.

KEYWORDS: Nanocomposite. Gel electrophoresis. Joule heating. Rheological properties

1 Introduction

Nanoparticles (NPs) have an extensive and significant impact on various fields of science.[1-3] Application of NPs have been extensively studied in separation science including microchip electrophoresis, liquid chromatography, gas chromatography, and capillary electrochromatography.[4,5] Polymer-based NPs were used to coat silica capillaries in capillary electrophoresis.[6-11] Silica gel NPs were also used as run buffer additive in capillary electrophoresis.[12] Surprisingly, very little research has been devoted to the application of NPs in slab gel electrophoresis. In this work, we demonstrate the use of ceria NPs to improve the resolution and efficiency of separation in slab gel electrophoresis.

Electrophoresis is a technique used to separate molecules that differ in size, charge, or conformation.[13,14] Polyacrylamide gel electrophoresis (PAGE) is one of the most powerful separation techniques for complex biological samples.[15] However, the efficiency and repeatability of the separation are limited by band broadening as a result of physical effects, which all are contributing to the spacial spreading of zones. Assuming Gaussian peak shapes, the broadness of bands can be expressed by the total variance, σ_t^2:

$$\sigma_t^2 = \sigma_D^2 + \sigma_J^2 + \sigma_A^2 + \sigma_O^2 \quad (1)$$

where the terms represent the variances due to the diffusion, Joule heating, adsorption, and other effects. The variance due to diffusion, σ_D^2, is related directly to the diffusion coefficient at time *t*:

$$\sigma_D^2 = 2Dt \quad (2)$$

The diffusion coefficient, *D*, is related to the ion radius, *r*, temperature, *T*, and viscosity of the solution, η via the Stokes-Einstein equation:[16]

$$D = \frac{kT}{6\pi\eta r} \quad (3)$$

where *k* is the Boltzmann constant. In electrophoresis, Joule heating is one of the most important factors in band broadening process. The heat produced, *q*, is directly proportional to the separation voltage, *V*; electric current, *I*; and time, *t*:

$$q = VIt \quad (4)$$

Reduction of Joule heating in slab gel electrophoresis is one of the most important goals to improve the separation efficiency. One approach is to apply lower voltages, when the Joule heating is the dominant contributor to band broadening, to improve the resolving power of the technique at the expense of increasing separation times. Capillary gel electrophoresis has resolved this issue by offering very high surface to volume ratio and efficient heat dissipation capability of the capillaries. Although the Joule heating and band broadening in slab gel electrophoresis is addressed by using capillaries but this happens at the expense of higher cost of the instrument and the loss of high throughput capability of slab gel electrophoresis. Single capillary gel electrophoresis suffers from low throughput whereas multiple capillary gel electrophoresis with high throughput capability is very expensive.

Suspending solid NPs into the gel is expected to improve heat transfer capability if the NPs have larger thermal conductivity than that of the gel itself. This improves the heat dissipation efficiency of the medium and changes the disadvantages of the slab gel electrophoresis to the advantages of capillary gel electrophoresis. Also, the much larger relative surface area of NPs improves significantly heat transfer capabilities of separation platforms.[17] Incorporation of dispersed inorganic NPs such as metal oxide NPs into a polymer matrix (gel), so-called polymer nanocomposites (PNCs), forms a smart gel with significant heat dissipation capability. The measurement of rheological properties of the PNCs provides useful guidelines to design and fabricate hydrogels with improved efficiency for protein separation in PAGE.

This work aims at the development of a gel incorporated with ceria NPs for improving the efficiency and speed of a sodium dodecyl sulphate polyacrylamide gel electrophoresis (SDS PAGE) separation of proteins. We focused on separation of standard proteins, a mixture of 14 recombinant, highly purified proteins. As an example of application, we also separated *E. coli* proteins without any attempt to identify the separated proteins. For the first time, we measured rheological parameters of gels and PNCs and observed a strong correlation with the improvement in separation. In other words, we measured rheological parameters of separation mediums in order to gain a better understanding of band broadening mechanism.

Theoretical calculations of the thermal conductivity and reduction in band widths of the protein separation well correlated with the results of rheological measurements. In fact, we took advantage of high throughput capability of slab gel electrophoresis and were able to lower the Joule heating in order to increase the speed of separation and improve the resolving power of the technique by incorporating ceria NPs in gel medium.

2 Experimental

2.1 Materials

All reagents were of analytical grade. Tris-hydroxymethylaminomethane (Tris), glycine, silver nitrate, *N*, *N*-methylenebisacrylamide (Bis), acrylamide, sodium dodecyl sulfate (SDS), ammonium persulfate (APS), sodium carbonate, mercaptoethanol, formaldehyde, tetramethylethylenediamine (TEMED), and sodium thiosulfate were purchased from Merck (Germany). Standard proteins and Coomassie Brilliant Blue (G-250) were purchased from Fermentas (PageRuler ^{TM}) and Sigma (USA) respectively.

2.2 SDS-PAGE

One-dimensional slab gel electrophoresis (Bio-Rad) of proteins was carried out in a 12 % vertical polyacrylamide (PA) gel (8 x 10 cm) containing sodium dodecyl sulphate according to the Laemmli protocol.[18] All samples were prepared in 5x concentrated Laemmli reducing buffer and boiled for 4 min before being used. Sample buffer (5x) contains Tris-HCl (1.0 mL, 0.125 M, pH 6.8), glycerol (1.0 mL, 20 %), SDS (1.5 mL, 10 %), mercaptoethanol (0.4 mL, 2 %) and bromophenolblue (0.2 mL, 0.05 %). Running buffer (5x) was prepared by mixing SDS (5.000 g), Tris (94.000 g), and glycine (15.100 g) adjusted with deionized water (1.00 L).

All solutions and buffers were filtered in order to remove dust particles. The protein concentrations of the samples were adjusted so that approximately 7 µL of standard proteins (0.02-0.05 mg/mL) to be loaded per lane. After electrophoresis, proteins were visualized using silver staining and Coomassie Blue. Gels were subsequently fixed overnight and silver stained (*E. coli* proteins). The standard proteins resolve into clearly identifiable sharp bands from 10 kDa to 200 kDa when analyzed by SDS-PAGE and stained with Coomassie Brilliant Blue (G-250). Gel images were analyzed using *ImageJ*[19] and *GelAnalyzer*[20] softwares. The digitization algorithm and the process of background subtraction is not discussed by the software company.

2.3 Gel staining

The solutions containing thiosulfate had to be freshly prepared in order to have sensitive and reproducible staining.[21] All steps of the silver staining procedure were performed in white plastic containers to facilitate the observation of image development. The silver staining method was reported elsewhere and we did not change the procedure.[5] In Coomassie Blue Staining**,** gels were stained and destained according to the standard protocol[22] which speeds up the destaining process for faster results with increased sensitivity for identifying proteins.

2.4 Preparation of ceria NPs

Cerium ammonium nitrate (3.65 mmol) was dissolved in deionized water (20 mL). The proper amount of NaOH solution (0.18 M) was added rapidly to the solution until the white precipitate was formed. The reaction vial was then placed into a microwave (Panasonic, model: NN-C2003S, Power: 800 W) in a cycling mode of 10 s ON and 5 s OFF (30 % power). The resulting precipitate was centrifuged (10 min with 13.000 rpm) and washed with deionized water several times. Finally, the products were dried in a vacuum oven at 60 °C overnight.[23,24]

2.5 Synthesis of PA/ceria nanocomposite hydrogel

PA/ceria nanocomposite hydrogel was synthesized by means of *ex situ* nanocomposite synthesis technique. Briefly, a proper amount (0.01-0.05 %) of ceria NPs was added to buffer (2.0 mL) and sonicated for 30 min at 30 °C in ultrasound bath. PA gel stock solution (30 %, m/v) was prepared by dissolving acrylamide (29.2000 g) plus Bis (0.8000 g) in H_2O (100.0 mL), and filtered. The 12 % gel solution was prepared by mixing gel stock solution (4.0 mL), Tris-HCl (2.5 mL, 1.5 mol L^{-1}, pH 8.80), $(NH_4)_2S_2O_8$ (100 µL, 10 %, m/v), TEMED (10 µL), SDS (100 µL), and ceria NPs (0.0020 g, 0.03 % w/v).

The gel solution used in this work was freshly prepared within 1 day of running the experiment. The gel solution containing ceria NPs was quite stable till the polymerization at room temperature (25 °C) indicating that the NPs were well dispersed in the gel medium.

2.6 Rheological measurement

The rheological measurements were performed on DV-II-Pro rheometer (Brookfield Instruments, USA). The cuvette (two concentric cylinders) cell geometry was used for monitoring the viscosity versus different shears. The rheometer is equipped with a thermo-bath with circulating water that was calibrated to give a temperature in the sample chamber within ±0.2 °C of the set value.

2.7 Characterization methods

X-ray diffraction measurements were determined by Bruker/D8 Advanced diffractometer in the 2θ range from 20° to 80°, by step of 0.04 degree, using graphite monochromatic Cu Kα radiation (λ= 1.541 Å). The TEM was carried out on an LEO 912 AB transmission electron microscope with the electron beam accelerating voltage of 120 kV.

3 Results and discussion

3.1 Characterization of prepared ceria NPs

Fig. 1a shows the XRD pattern of the ceria NPs. The diffraction peaks could be assigned to the (111), (200), (220), (311), (222), (400), (331), and (420) planes which are indexed to the face-centred cubic phase with the lattice parameter of $a = b = c = 0.5410$ nm. Obviously, there is no additional peak in the XRD pattern of sample which can be attributed to the high purity of the prepared ceria NPs. The strong and sharp peaks indicate the good crystallinity of the NPs. According to the results, the average grain size for the sample was 3.5 nm. TEM image of prepared ceria NPs is shown in Fig. 1b. The nanoparticles display the uniform cubic morphology with the average size of about 3 nm which are in a good agreement with the results deduced from XRD.

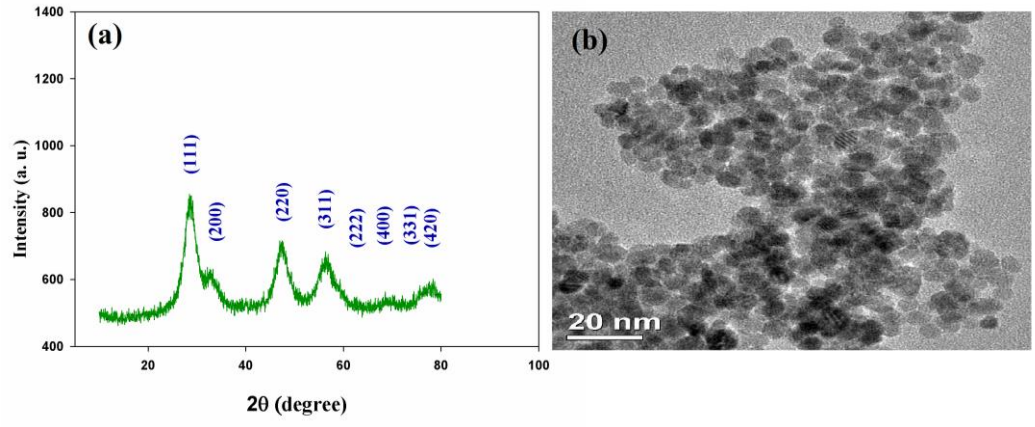

Fig. 1 (a) The XRD pattern and (b) The TEM image of prepared ceria NPs.

3.2 Rheological studies

Rheology of PA solution and PA/ceria suspensions were measured in order to promote a fundamental understanding of the band broadening and to investigate the influence of ceria NP inclusion on rheological properties of PA solution. Fig. 2 (a, b, and c) shows the viscosity of the PA solution and PA/ceria suspensions as a function of shear rate, γ^{o} (rate of deformation) at different temperatures. The reduction of viscosities arising from the incorporation of ceria NPs in the PA solution was observed in contrary to the predictions by Einstein [25] (equation 5) but in agreement with Mackay *et al*:[26]

$$\eta = \eta_0(1+C\phi) \qquad (5)$$

where η_o and η stand for the viscosity of the PA gel and PA/ceria suspension with the volume fraction of ϕ, and C is a constant. For a given weight fraction of the NPs suspension in a gel matrix, W, the volume fraction is defined as:

$$\phi = \frac{W}{W + (1-W)\frac{\rho_n}{\rho_m}} \qquad (6)$$

where ρ_n and ρ_m are the densities of the NPs and matrix, respectively. The Einstein equation may be an accurate representation of the behavior of the suspensions over only a vanishingly small range of solid concentrations. The initial decrease in viscosity of polymer solution by incorporating the NPs may be attributed to the change of the free volume caused by the NPs.[26] A maximum of 43 % decrease in viscosity of PA solution at 25 $^{\circ}$C and shear rate of 19.8 s^{-1} was observed when 0.05 % w/v of ceria NPs was added into PA solution. Also, by loading 0.03 % w/v of ceria NPs at 25 $^{\circ}$C and shear rate of 19.8 s^{-1}, the viscosity of PA solution decreased by 22 %.

As Fig. 2 (a, b, and c) shows at shear rates near zero, both PA solution and PA/ceria suspensions have high viscosity due to random orientations of the molecules.[27] Also, the initial viscosity

increased with ceria NPs loading for shear rates near zero at 25 °C (Fig. 2a). This effect is eliminated at higher temperatures (Fig. 2b and c). The initial increase in viscosity with NPs loading at 25 °C is due to the higher interfacial interaction between the components at the interface.[28] Both in PA solution and PA/ceria suspensions, the viscosity decreased with increase of shearing indicating a pseudoplastic behavior. By applying shearing force, the polymer chains are oriented resulting in the reduction of shear viscosity and thus exhibited non-Newtonian pseudoplastic behavior. The non-Newtonian behavior is more prominent at higher ceria NPs loadings. As the NPs loading increases, the shear viscosity decreases. The decrease might be associated with the formation of micelles (NPs clusters might form micelles) which had a plasticizing action on the viscosity of the PA solution.[29] At shear rates approximately greater than 30 s^{-1}, the viscosity of both the neat polymer solution and the nanocomposite reached a plateau value namely Newtonian behavior. Interestingly, at high shear rates, the viscosities become irrelevant to the concentration of ceria NPs and appear to converge toward a Newtonian plateau.

Fig. 2 shows the viscosity of PA/ceria suspensions is always less than that of PA solution under the same conditions irrespective of the value of shear rate. Hence, if we assume the electric field in electrophoresis applies a shearing force on the system of interest, it is plausible to say that the viscosity of PA/ceria suspensions is always less than that of PA solution. Considering band broadening due to the diffusion (Equation 2), reduction in viscosity causes increase in diffusion coefficient which is counterbalanced by decreased migration time of proteins. Shear flow curves of the PA solution and PA/ceria suspensions (Figs. 2d, e, and f) showed reasonably straight lines and obeyed the Ostwald‑de Waele equation:[30]

$$\tau = K(\gamma^{o})^{n} \quad (7)$$

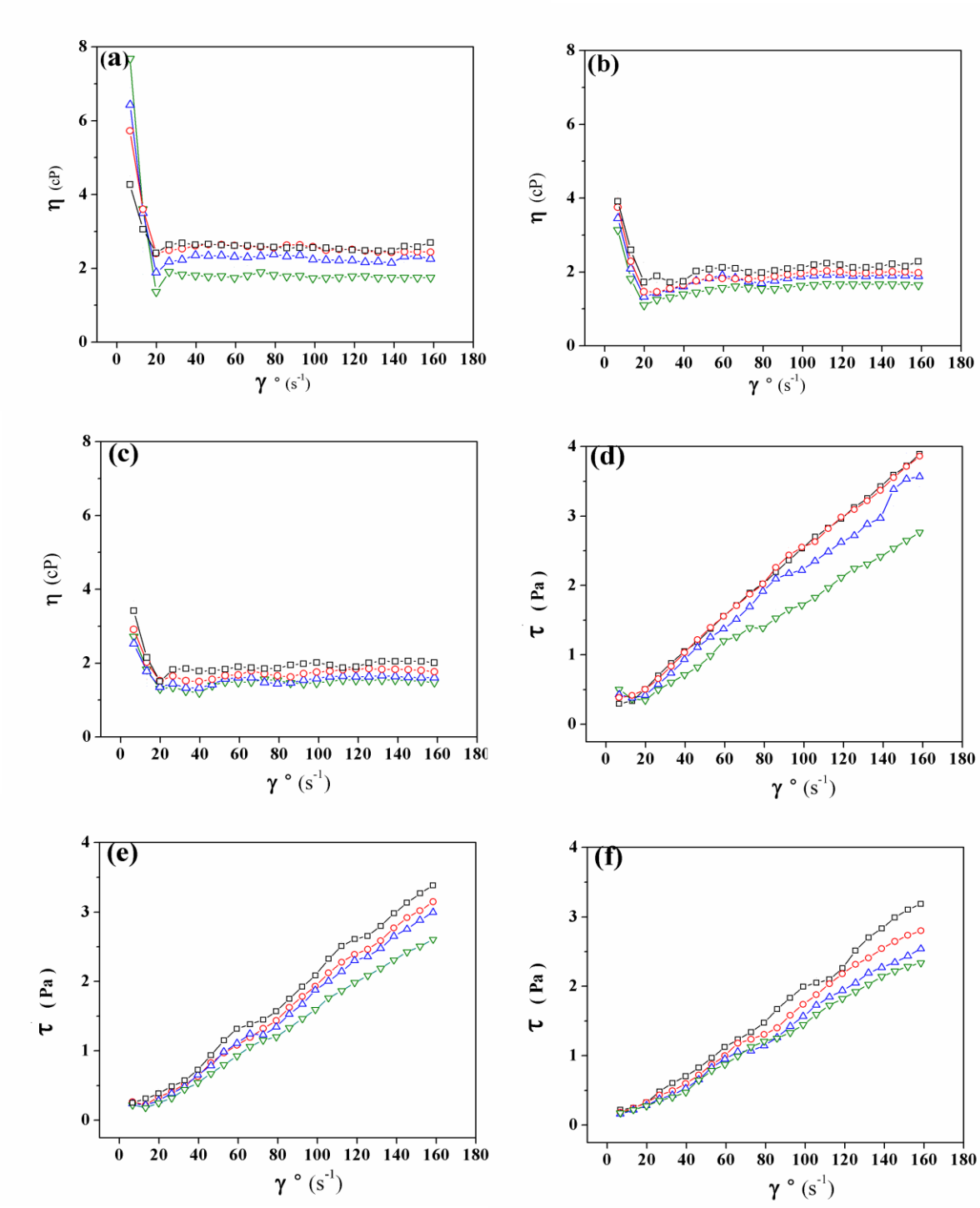

Fig. 2 Viscosity curves for PA solution and PA/ceria suspensions at (a) 25, (b) 35, and (c) 45 °C. The shear flow curves for the PA solution and PA/ceria suspensions at (d) 25, (e) 35, and (f) 45 °C (PA solution, PA/ceria (w/v % = 0.02), PA/ceria (w/v % = 0.03), PA/ceria (w/v % = 0.05)).

where τ, and n are shearing stress and the power law index or the flow behavior index. K stands for consistency of the flow or viscosity coefficient index. Table 1 shows the power law index and the viscosity coefficient index for PA solution and PA/ceria suspensions at different temperatures. The shear flow curves for both PA solution and PA/ceria suspensions illustrates the pseudoplastic property as shear thinning behavior, i.e. the apparent shear viscosity of the two sets of blends decreased as the shear rate increased (Fig. 2).

Table 1 The power law index and the viscosity coefficient index for PA solution and PA/ceria suspensions at different temperatures.

w/v %	*n* (kPa)	*K*	R^2
T=25 °C			
0.00	0.945	33.1	0.999
0.02	0.925	35.2	0.997
0.03	0.951	36.2	0.991
0.05	0.916	26.2	0.986
T=35 °C			
0.00	1.047	17.0	0.995
0.02	1.099	12.1	0.997
0.03	1.080	12.8	0.996
0.05	1.091	10.5	0.997
T=45 °C			
0.00	1.090	12.1	0.997
0.02	1.083	12.2	0.996
0.03	1.078	11.0	0.996
0.05	1.043	12.3	0.996

3.3 Band broadening

The ratio of the values of $\sigma_D{}^2$ for the PA/ceria (PAC) suspensions to PA solution is obtained by using Equations 2 and 3:

$$\frac{(\sigma_D{}^2)_{PAC}}{(\sigma_D{}^2)_{PA}} = \frac{T_{PAC}}{T_{PA}} \times \frac{\eta_{PA}}{\eta_{PAC}} \times \frac{t_{PAC}}{t_{PA}} \quad (8)$$

where t_{PA} and t_{PAC} stand for separation time in PA solution and PA/ceria suspensions, respectively. T_{PA} and T_{PAC} refer to separation medium temperatures for the PA solution (45 $^{\circ}$C) and PA/ceria (35 $^{\circ}$C) suspensions, respectively. There are three factors affecting the ratio of variances of PA/ceria suspensions to PA solution: $\frac{T_{PAC}}{T_{PA}}$, $\frac{t_{PAC}}{t_{PA}}$, and $\frac{\eta_{PA}}{\eta_{PAC}}$ which are less than one for the first and the second and greater than one for the third factor, respectively. The overall multiplication of these three parameters is lower than one; indicating that band broadening due to diffusion for the PA/ceria suspensions is less than that of PA solution. This indicates that incorporation of ceria NPs into PA gel matrix lowers diffusion coefficient and hence lowers the band broadening. Table 2 gives the ratio of diffusion variations for the PA/ceria suspensions to PA solution at two different shear rates. We performed separation with PA solution and PA/ceria suspensions at the same starting temperature. At shear rate 72.6 s^{-1}, by increasing the loading of 0.02 w/v % ceria NP, $\frac{(\sigma_D)_{PAC}}{(\sigma_D)_{PA}}$ increased from 0.944 to 0.998 in 0.05 w/v % of ceria NP. Although this variation is subtle but it is important because it shows diffusion coefficient in PA/ceria suspension increases by increasing NP loading. For calculation of diffusion variations, the viscosity and temperature of the PA solution and PA/ceria suspensions was measured at different shear rates and different NP concentrations. The $\frac{(\sigma_D)_{PAC}}{(\sigma_D)_{PA}}$ values were measured according to Equations 2 and 3. The separation medium

temperature for PA/ceria reduces because ceria NPs act as heat sink and hence the band broadening decreases (see next section). The viscosity for the PA solution and PA/ceria suspensions was also measured at the temperatures of separation medium.

Fig. 3 displays a series of *I*-*V* measurements for the PA gel and the PA/ceria gel. The Joule heating disrupts the separation process at the threshold of nonlinearity in the *I*-*V* curve and this happens when the rate of heat generation by Joule heating surpasses the rate of heat dissipation by the gel medium. The ceria NPs act as heat sinks and increase the rate of heat dissipation. Separation power increases with increase in applied voltage (*V*). However, the increased voltage is converted into Joule heating through the frictional drag of the various ionic species forced along the conducting pathways. Excess heat will melt the separation medium (gels), increase the tendency for convection, decompose heat-sensitive molecules, cause the evaporation of volatile components and of water, and increase migration rate in a rather non-uniform manner.

A threshold voltage (V_t) above which the current begins to abruptly increase is the maximum separation voltage that should be applied in order to having the shortest separation time. The values of V_t in the pure PA gel and the PA/ceria gel were measured to be 150 and 200 V, respectively. As Fig. 3b shows, at high voltages, Joule heating for the PA/ceria gel is less than that of the PA gel (Equation 4). Fig. 3b shows the calculated Joule heating for both the PA solution and PA/ceria suspensions at different applied voltages. As this figure shows by incorporating the ceria NPs in the PA solution, the amount of Joule heating decreases. By increasing ceria NPs loading, the magnitude of Joule heating decreases further. The decrease of the Joule heating with the loading of the ceria NPs in the PA solution might be associated with the decrease in viscosity as the rheological studies showed.

We chose ceria NPs because of having both high thermal conductivity and low electrical conductivity (0.044 S m^{-1}).[31] The thermal conductivity of ceria NPs (19 W m^{-1} K^{-1})[32] is 34 times higher than that of PA (0.56 W m^{-1} K^{-1}).[33] There are reports on incorporating CNTs into PA gels to improve the resolutions of human serum proteins.[34,35] CNTs have not only high thermal conductivity (3500 W m^{-1} K^{-1})[36] but also high electrical conductivity (10^6-10^7 S m^{-1}).[37] This causes the CNTs move when the separation voltage is applied and create a viscosity gradient with higher viscosity zones depleted from CNTs and lower viscosities in zones that CNTs have moved into. This viscosity gradient causes a gradient in migration time and hence band broadening.

Table 2 The ratio of diffusion variations for the PA/ceria suspensions to PA solution.

w/v %	$\frac{(\sigma_D)_{PAC}}{(\sigma_D)_{PA}}$
γ^o = 72.6 s^{-1}	
0.02	0.94
0.03	0.96
0.05	1.00
γ^o = 145.2 s^{-1}	
0.02	0.95
0.03	0.97
0.05	0.99

The Joule heating would be lower on the side where the CNTs have migrated to and higher on the depleted side. There are no theoretical formulas currently available to predict the thermal

conductivity of the NPs suspensions, so-called nanofluid, satisfactorily.[38] The Maxwell model,[39] an existing traditional model for thermal conductivity, was proposed for solid–liquid mixtures with relatively large particles:

$$\lambda_c = \frac{\lambda_f + 2\lambda_m + 2\phi(\lambda_f - \lambda_m)}{\lambda_f + 2\lambda_m - \phi(\lambda_f - \lambda_m)} \quad (9)$$

where λ_c, λ_f, and λ_m are the thermal conductivities of PA/ceria suspension, ceria NPs, and PA, respectively. The thermal conductivities of PA/ceria suspensions was calculated based on Maxwell model as 1.0037, 1.0074, 1.0114 and 1.0194 for 0.01, 0.02, 0.03, and 0.05 w/v % of ceria NPs, respectively. This is equivalent to 79, 80, 81 and 82 % enhancement in thermal conductivities as compared with thermal conductivity of PA gel with no ceria NPs. By loading the ceria NPs in PA solution, the thermal conductivity increases. It should be mentioned that the Maxwell's formula underestimates the thermal conductivity of PA/ceria suspension, i.e. the thermal conductivity of PA/ceria suspension is much higher than that of predicted by this model. The Maxwell model predicts the effective thermal conductivity of liquid-solid mixtures for low volume concentration of spherical particles. When the particle concentration is sufficiently high or the size of particles lies in submicron domain, the Maxwell model fails to provide a good match with the experimental results. As Fig. 3b shows by incorporating the ceria NPs in the PA solution, the amount of Joule heating decreases. At applied voltage of 160 V, by loading 0.01 and 0.03 w/v % of the ceria NPs, the value of Joule heating decreases 9 % and 18 %, respectively, as compared to that of PA solution. At 200 V, these values become 12 % and 35 %, respectively. Joule heating decreases by incorporation of ceria NPs and this leads to reduction of both temperature gradient and uneven migration in the gel. By performing the PA gel at 200 V with no ceria NP incorporation, the migration time lowered

from 100 min to 65 min, but the excess Joule heating generated causes severe band broadening and loss of efficiency (see Figs .3a and 3b).

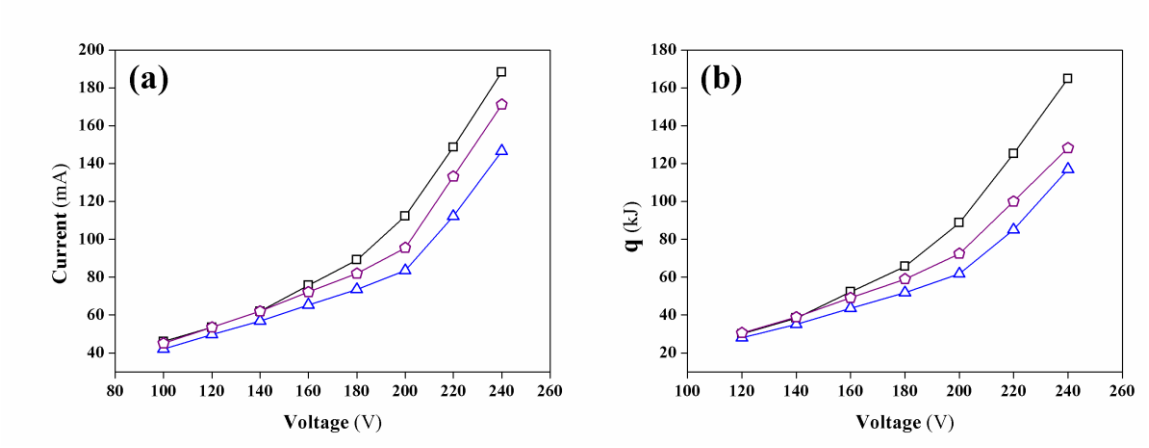

Fig. 3 (a) Current *vs* voltage curve for the PA gel and PA/ceria gel (b) The magnitudes of Joule heating versus applied voltage for PA gel and PA/ceria gels (PA solution, PA/ceria (w/v % = 0.01), PA/ceria (w/v % = 0.03)).

3.4 SDS-PAGE of protein mixtures

3.4.1 Separation of proteins on PA/ceria nanocomposite gel

The gel images and electropherograms of standard proteins (a mixture of 14 recombinant, highly purified proteins ranging from 10 kDa to 200 kDa) on PA and the PA/ceria gels are shown in Fig. 4. The gel images were digitized and converted to the electropherograms. Separation of proteins was performed at two different voltages (150 and 200 V) which were chosen based on the Joule heating threshold voltages for PA and the PA/ceria gels. At first, proteins were separated using both PA gel and PA/ceria gels at Joule heating threshold voltage for PA (150 V) (Fig. 4a and b). Then, separation was repeated at the same conditions but running at 200 V threshold voltage for PA/ceria gels (Figs. 4c and d). Comparing Fig. 4e (gels run at 150 V) with Fig. 4f (gels run at 200 V) shows that migration time of proteins were reduced in PA/ceria gel compared to the PA gel. By performing the electrophoresis at threshold Joule heating voltages of 150 V and 200 V for PA and PA/ceria

gels, the migration time decreased from maximum 100 minutes to 60 minutes, respectively. Inclusion of ceria NPs into the PA gel, expanded the applicable voltage to 200 V and therefore deceased migration times of proteins. For example, as it can be seen in Figs. 4e and 4f, the migration time of standard proteins (60 kDa) was decreased from 33 min in PA gel at 150 V to 12 min in PA/ceria gel at 200 V.

By incorporating the ceria NPs, the migration time of proteins increases as compared with the pure PA gel at the same applied voltage (Figs. 4e and 4f). For example, migration time of protein (50 kDa) was increased 4 % and 7 % at 150 V and 200V, respectively. The inclusion of ceria NPs modifies the PA gel pore size distribution. At the same time, as the results of rheological measurements show (section 3.2), ceria NP lowers the viscosity of PA gel. While these two effects partially counterbalance each other, it seems that the pore size modification might have slightly higher effects to cause this increase in migration times at constant voltage. The efficiency of the electrophoretic system was calculated by the number of theoretical plates, N:[40]

$$N = 5.54\left(\frac{t}{w_{1/2}}\right)^2 \quad (10)$$

where t and $w_{1/2}$ stand for migration time of the protein and the temporal peak width at half of the peak height. The number of theoretical plates for the defined peaks (A to O), in both PA and PA/ceria gels was measured (Equation 10). It was observed that the value of N increased in PA/ceria gel compared to that of PA gel. For example, the sharpness and value of N for peak I increased 32 % in 150 V and 48 % in 200 V in PA/ceria gel compared to the PA gel. For separation at 200 V, the number of theoretical plates for peaks H to M in PA/ceria gel increased 78, 46, 73, 36, 17, and 24 percent, as compared with PA gel (see Figs. 4c and 4d). This is a clear indication of improvement in separation efficiency. Furthermore, the number of separated peaks increased in PA/ceria gel and peaks split into more peaks (peaks AB and F in PA gel split into peaks A_1, A_2, B,

F_1, and F_2 in PA/ceria gel, 200 V, see Figs. 4c and 4d). The number of theoretical plates N is related to the applied voltage, V, effective charge, z, the Faraday constant, F, temperature, T, and gas constant, R via the following equation:[41]

$$N = \frac{z\,FV}{2\theta RT} \tag{11}$$

where θ is dispersion coefficient. In electrophoresis, efficiency N is maximized by increasing voltage V as far as Joule heating allows. By incorporation of ceria NPs into the PA gel, it would be possible to expand the Joule heating threshold voltage. In separation at 150 V (Figs. 4a and 4b), the number of theoretical plates for the peaks (H to M) increased in PA/ceria gel (Fig. 4b) as compared with PA gel (Fig. 4a). For example, the number of theoretical plates for peaks H to M in PA/ceria gel (Fig. 4b) increased up to 12, 32, 56, 27, 8, and 19 percent, respectively. This indicates that the separation efficiency has increased when the NPs were embedded in the gel matrix. These improvements in separation efficiency are correlated with the decrease in Joule heating (Fig. 3b).

The resolution R_s is also another important index of success for the analytical separation of two specific components. The resolution between two peaks in electropherograms can be calculated as follows:[40]

$$R_s = \frac{2(t_2 - t_1)}{w_1 + w_2} \tag{12}$$

where t_1 and t_2 are the migration times for components 1 and 2, respectively. w_1 and w_2 stand for the temporal peak width of components 1 and 2, respectively. The appropriate resolution between components requires a combination of good selectivity reflected in incremental velocity and good system efficiency (narrow peaks) and in N ($R_s \sim N^{1/2} \sim V^{1/2}$).[42,43] Thus, resolution should improve by enhanced efficiency and higher applied voltages. Resolution between bands increased in PA/ceria gel compared with pure gel. Comparing Fig. 4a with Fig. 4d shows the resolution between

bands HI and JK increased 69 and 53 percent, respectively (see Table 3). The resolution between bands L and M improved from 2.11 in PA gel (Fig. 4a) at 150 V to 4.98 in PA/ceria gel at 200 V (Fig. 4d). The overall resolution, almost improved for all the peaks in ceria modified gels as compared with PA gel (Table 3). At 150 V, the resolution between bands increased in ceria modified gels compared to pure gel (Figs. 4a and 4b). The resolution between bands HI and JK increased 15 and 35 percent, respectively.

Table 3 Resolution measurements for selected bands for PA and PA/ceria gels at 150 and 200 V.

Peak	R_s			
	PA gel		PA/ceria gel	
	150 V	**200 V**	**150 V**	**200 V**
HI	1.12	0.98	1.29	1.56
JK	1.61	1.50	2.18	2.30
LM	2.11	4.51	2.15	4.98

By embedding ceria NPs into the matrix, the pore size distribution of matrix changes and this leads to pore size modification of pure gel. This modification might be negligible because only 0.03 w/v % of ceria NPs was used. As the nanofiller size decreases, the pore density increases compared to that of unfilled polymeric matrix.[44,45] The increase in migration time of proteins in PA/ceria gels compared to PA gel might be an indication of pore size modification in the presence of ceria NPs.

There are three parameters that should be considered when comparing the band broadening and its improvement in PA/ceria gel; (1) modification of pore size, (2) lowering the viscosity, and (3) increasing thermal conductivity. Considering low percentage of ceria NPs (0.03 %), the pore size modification should be partially counterbalanced with decrease in viscosity (22 % based on

rheology calculation). Hence, the main parameter in favor of lowering Joule heating is thermal conductivity increase (81 %).

If ceria NPs would act as nanofiller to modify the pore size distribution of PA gel, a similar increase in migration times would be expected. Comparing Fig. 4a (PA gel at 150 V) with Fig. 4b (PA/ceria gel at 150 V), there is no significant change in migration times. Including low amount of ceria NP (0.03 % w/v) in gel, the pore size modification should be very low if not negligible. The increase in migration time might be counterbalanced with lowering the viscosity when including NPs into the PA gel. The changes in migration time of standard proteins in PA and PA/ceria gel (Figs. 4e and 4f, the PA gel with and without ceria NPs both performing at the same voltage) may be due to pore size modification.

In general, the sharpness and resolution of all defined bands increased in ceria modified gel because the NPs alter both the pore size distribution and thermal conductivity of polymer matrix. By embedding ceria NPs into the matrix, the pore size distribution of matrix changes and this leads to changes to the pure gel. Incorporation of ceria NP which is distributed uniformly inside gel matrix causes: (1) increasing the Joule heating threshold voltage from 150 V to 200 V. This leads to (a) lowering migration time (lower longitudinal diffusion at higher voltages) and (b) lowering the viscosity. These two phenomena counteract each other. (2) The unique distribution of NPs will cause uniform dissipation of heat and multiple heat center sites distributed uniformly across the gel. Thus, it lowers the uneven distribution of migration and causes the sharpness of peaks. Indeed when ceria NPs are embedded in PA gel and the applied voltage is increased from 150 V to 200 V, the $W_{1/2}$ lowers slightly from 2.3 to 2.2 and this causes the peak O, for example, to be sharper. Based on equation 11, we expect running the gel at 200 V to produce a peak with higher N (and higher peak intensity) as compared with the experiments performed at 150 V. Although, we observe the increase

in band intensity both with and without NPs when the separation voltage is increased, but the degree of contribution from other parameters such as increase in T or the effect of higher temperatures to lower the viscosity and, therefore, increase the θ is not well understood.

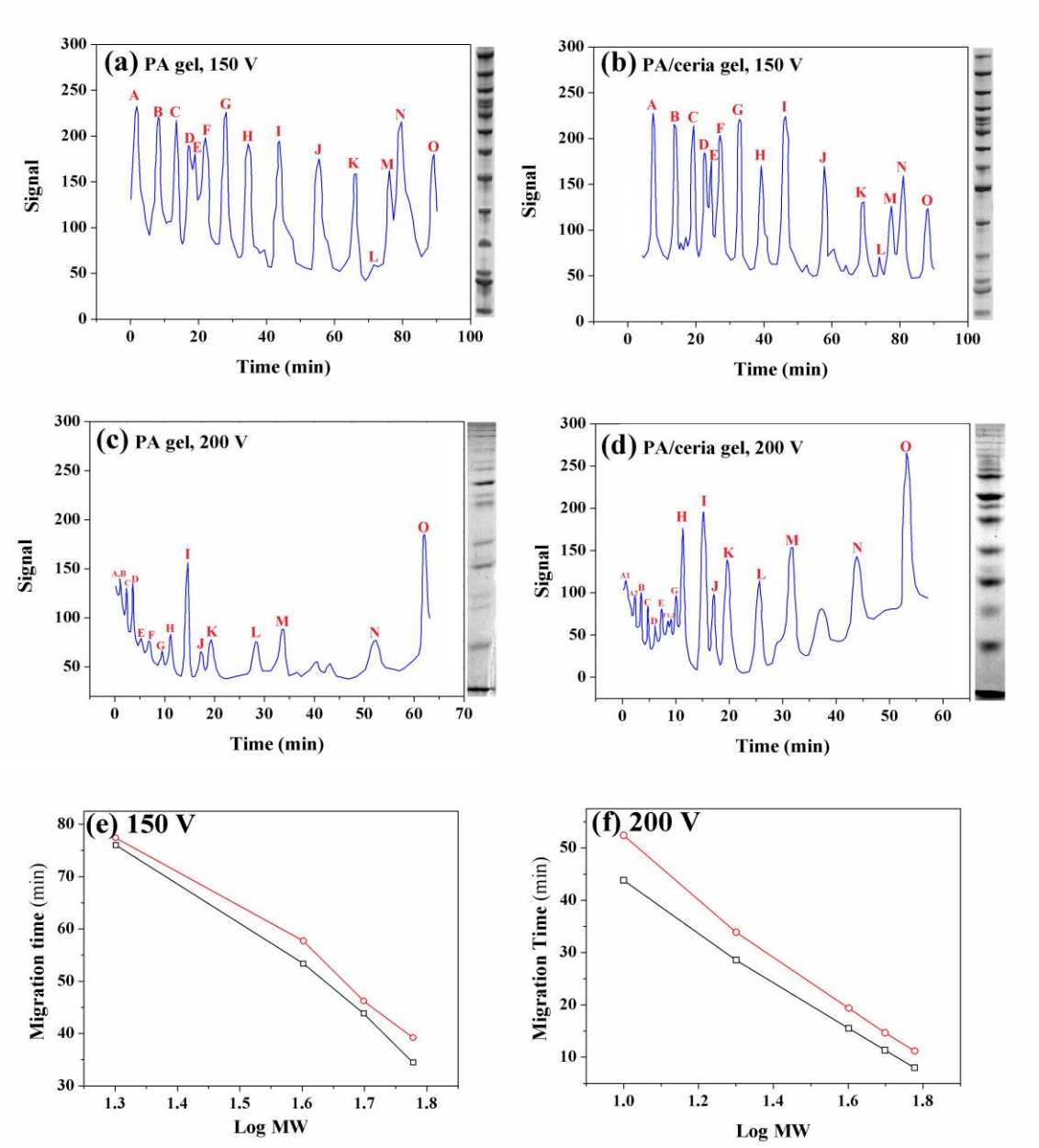

Fig. 4 The electropherograms of standard protein sample on the (a) PA gel at 150 V (b) PA/ceria gel at 150 V and (c) PA gel at 200 V (d) PA/ceria gel at 200 V. The migration time of standard protein sample versus molecular weights at (e) 150 V (f) 200 V (-□- PA gel, -○- PA/ceria gel).

3.4.2 Separation of *E. coli* proteins on PA/ceria nanocomposite gel

As an example of application, we separated *E. coli* proteins. Separation was performed on the pure PA and PA/ceria gels in order to compare the efficiency of separation without any attempt to characterize the separated proteins. The separation panels and electropherograms of *E. coli* proteins on PA and the PA/ceria gels are shown in Fig. 5. The separation was carried out at 150 V. The number of theoretical plates for the peaks A to I for both PA and PA/ceria (w/v= 0.03 %) gels was measured. It was observed that the value of *N* increases in PA/ceria gel (Fig. 5b) compared to that of PA gel (Fig. 5a). For example, the value of *N*, for peaks A, B, C, F, G, H, and I in PA/ceria gel increased by 11, 43, 65, 221, 53, 64, and 78 percent, respectively compared to the PA gel. Also, the peak D splits into D_1 and D_2 peaks in PA/ceria gel. This is a clear indication of the improvement in separation efficiency when the NPs are embedded in the gel matrix. It seems that incorporation of ceria NPs to the gel increases the contrast that causes the signal enhancement. Resolution between peaks was also measured in PA/ceria and PA gels. In general, the resolution increased in PA/ceria gel compared to that of the PA gel alone. For example, the resolution between peaks H and I for both PA and PA/ceria gels was of 1.09 and 1.60, respectively. Hence, the resolution increased up to 47 % in PA/ceria gel.

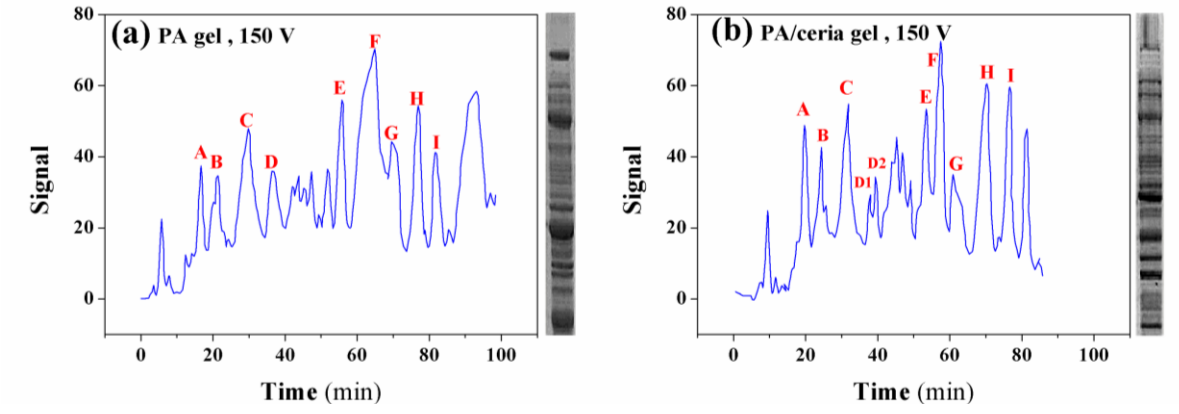

Fig. 5 The gel images and separation electropherograms of *E.coli* protein on the (a) PA gel (b) PA/ceria gel at 150 V.

3.5 Influence of ceria NPs concentration

In order to understand the relationship between ceria NPs concentration and the degree of improvement in separation parameters, different concentrations of ceria NPs (0.01, 0.03, and 0.05 w/v %) were incorporated into PA gel. When the concentration of ceria NPs was set at 0.01 w/v %, no obvious change was observed. The optimum separation efficiency was obtained for 0.03 w/v % of ceria NPs. However, when the concentration of the ceria NPs was higher than 0.03 w/v %, no significant improvement in separation parameters was achieved. In silver staining of gels, the excess ceria NPs interferes with stained gel (Pale yellow) which increases the background of silver staining images but lowers the *S/N* ratio for Coomassie Blue (G-250) staining. The ceria NPs increased the *S/N* ratio and better images were obtained. Fig. 6 shows that for images of Coomassie Blue stained PA/ceria gel, the peak pixel values were distributed over the bigger gray value ranges. It confirms the fact that PA/ceria gel image has a higher contrast compared to that of PA gel (narrow peak). It is an indication of better contrast in PA/ceria gel. The mean value with its standard deviation in PA/ceria gel image is 179 ± 2, whereas for PA gel is 214 ± 1 (histogram prepared by *ImageJ*).

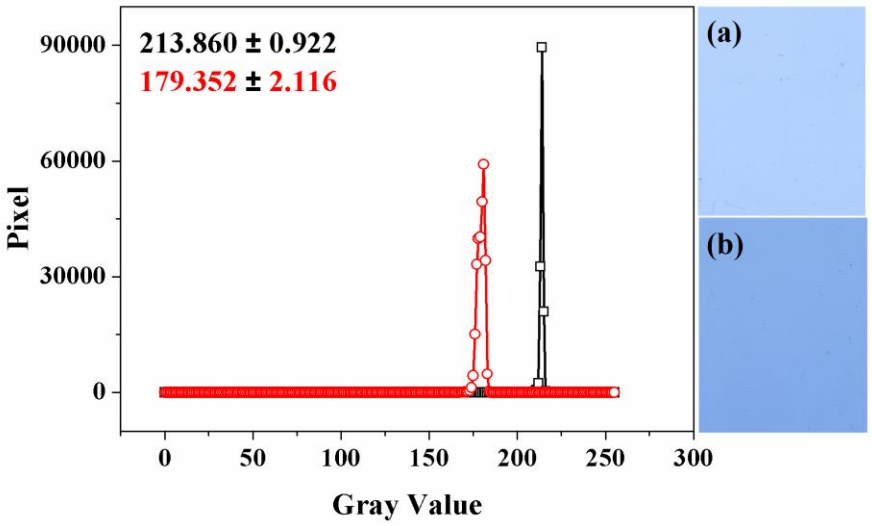

Fig. 6 Histogram of (a) PA (□) and (b) PA/ceria (○) gels (pixel intensity versus gray values).

4 Conclusions

In summary, ceria NP embedded PAGE could improve the analytical figures of merit by reducing Joule heating and lowering the band broadening. In order to understand the relationship between the ceria NPs concentration and the degree of improvement in separation parameters, different concentrations of ceria NPs (0.01, 0.03, and 0.05 w/v %) were incorporated into PA gel. The optimum separation efficiency was obtained for 0.03 w/v % of ceria NPs. The influence of rheology on the effect of Joule heating was successfully evaluated and the attenuation of Joule heating effect was observed by dispersing the ceria NPs in the PA solution.

We developed a general framework to compute the thermal conductivity of ceria NPs suspended in PA solution. By loading 0.03 % w/v ceria NPs in PA solution at 25 $^{\circ}$C, the viscosity decreased 22 % and thermal conductivity increased 81 %, which resulted in 35 % reduction in Joule heating and 56 % increase in separation efficiency. As far as we know, this is the first report on using NPs to improve the separation figures of merit by taking advantages of high throughput capability of slab gel electrophoresis and the high heat dissipation efficiency, resolution, and number of theoretical plates in single capillary gel electrophoresis.

Finally, this paper presents a future potential to improve the separation efficiency and resolution of other proteins using PAGE. Further work to validate the results reported in this article is in progress with other oxide NPs and the results will be communicated in future contributions.

Acknowledgements

The authors acknowledge Ferdowsi University of Mashhad for supporting this project (3/23032). HA thanks ATF committee for financial support. The authors also thank Dr. Sara Samiee for preparation of ceria NPs.

References

1 Martin, C. R., Mitchell, D. T. Nanomaterials in analytical chemistry. *Analytical Chemistry* **70**, 322A-327A (1998).

2 Godovsky, D. Y. in *Biopolymers· PVA Hydrogels, Anionic Polymerisation Nanocomposites* 163-205 (Springer, 2000).

3 Schmidt, G. & Malwitz, M. M. Properties of polymer–nanoparticle composites. *Current Opinion in Colloid & Interface Science* **8**, 103-108 (2003).

4 Yang, L. *et al.* Gold nanoparticle-modified etched capillaries for open-tubular capillary electrochromatography. *Analytical Chemistry* **77**, 1840-1846 (2005).

5 Nilsson, C. & Nilsson, S. Nanoparticle-based pseudostationary phases in capillary electrochromatography. *Electrophoresis* **27**, 76-83 (2006).

6 Kleindienst, G., Huber, C. G., Gjerde, D. T., Yengoyan, L. & Bonn, G. K. Capillary electrophoresis of peptides and proteins in fused-silica capillaries coated with derivatized polystyrene nanoparticles. *Electrophoresis* **19**, 262-269 (1998).

7 Gelfi, C. *et al.* Surface modification based on Si-O and Si-C sublayers and a series of N-substituted acrylamide top-layers for capillary electrophoresis. *Electrophoresis* **19**, 1677-1682 (1998).

8 Huber, C. G., Premstaller, A. & Kleindienst, G. Evaluation of volatile eluents and electrolytes for high-performance liquid chromatography–electrospray ionization mass spectrometry and capillary electrophoresis–electrospray ionization mass spectrometry of proteins: II. Capillary electrophoresis. *Journal of Chromatography A* **849**, 175-189 (1999).

9 Rodrıguez, S. A. & Colón, L. A. Investigations of a sol–gel derived stationary phase for open tubular capillary electrochromatography. *Analytica Chimica Acta* **397**, 207-215 (1999).

10 Rodriguez, S. A. & Colón, L. A. Study of the solution in the synthesis of a sol-gel composite used as a chromatographic phase. *Chemistry of Materials* **11**, 754-762 (1999).

11 Strege, M. A. & Lagu, A. L. *Capillary Electrophoresis of Proteins and Peptides*. Vol. 276 (Springer, 2004).

12 Fujimoto, C. & Muranaka, Y. Electrokinetic chromatography using nanometer-sized silica particles as the dynamic stationary phase. *Journal of High Resolution Chromatography* **20**, 400-402 (1997).

13 Ahmadzadeh, H., Johnson, R. D., Thompson, L. & Arriaga, E. A. Direct sampling from muscle cross sections for electrophoretic analysis of individual mitochondria. *Analytical Chemistry* **76**, 315-321 (2004).

14 Ahmadzadeh, H., Dua, R., Presley, A. D. & Arriaga, E. A. Automated analysis of individual particles using a commercial capillary electrophoresis system. *Journal of Chromatography A* **1064**, 107-114 (2005).

15 Hames, B. D. *Gel Electrophoresis of Proteins: A Practical Approach: A Practical Approach*. Vol. 197 (Oxford University Press, 1998).

16 Petersen, N. J., Nikolajsen, R. P., Mogensen, K. B. & Kutter, J. P. Effect of Joule heating on efficiency and performance for microchip-based and capillary-based electrophoretic separation systems: A closer look. *Electrophoresis* **25**, 253-269 (2004).

17 Yi, P., Awang, R. A., Rowe, W. S., Kalantar-zadeh, K. & Khoshmanesh, K. PDMS nanocomposites for heat transfer enhancement in microfluidic platforms. *Lab on a Chip* **14**, 3419-3426 (2014).

18 Laemmli, U. K. Cleavage of structural proteins during the assembly of the head of bacteriophage T4. *Nature* **227**, 680-685 (1970).

19 Abràmoff, M. D., Magalhães, P. J. & Ram, S. J. Image processing with ImageJ. *Biophotonics International* **11**, 36-43 (2004).

20 I. Lazar, I. Lazar, Gel Analyzer 2010a: Freeware 1D Gel Electrophoresis Image Analysis Software, 2012.

21 Blum, H., Beier, H. & Gross, H. J. Improved silver staining of plant proteins, RNA and DNA in polyacrylamide gels. *Electrophoresis* **8**, 93-99 (1987).

22 Simpson, R. J. Rapid coomassie blue staining of protein gels. *Cold Spring Harbor Protocols* **2010**, pdb. prot5413 (2010).

23 Goharshadi, E. K., Samiee, S. & Nancarrow, P. Fabrication of cerium oxide nanoparticles: characterization and optical properties. *Journal of Colloid and Interface Science* **356**, 473-480 (2011).

24 Samiee, S. & Goharshadi, E. K. Effects of different precursors on size and optical properties of ceria nanoparticles prepared by microwave-assisted method. *Materials Research Bulletin* **47**, 1089-1095 (2012).

25 Liu, J., Zhang, L., Cao, D. & Wang, W. Static, rheological and mechanical properties of polymer nanocomposites studied by computer modeling and simulation. *Physical Chemistry Chemical Physics* **11**, 11365-11384 (2009).

26 Mackay, M. E. *et al.* Nanoscale effects leading to non-Einstein-like decrease in viscosity. *Nature Materials* **2**, 762-766 (2003).

27 Block, R. J. *A Laboratory Manual of Analytical Methods of Protein Chemistry*. Vol. 2 (Pergamon Press, 1960).

28 Thomas, S., Chan, C. H., Pothen, L. A., Rajisha, K. & Maria, H. *Natural Rubber Materials: Volume 1: Blends and IPNs*. Vol. 7 (Royal Society of Chemistry, 2013).

29 Boochathum, P. Rheological Behaviour of Natural Rubber Based Blends. *Natural Rubber Materials: Volume 1: Blends and IPNs* **7**, 394 (2013).

30 Han, C. D. Rheology in polymer processing. Academic Press, 1976.

31 Rupp, J. L. & Gauckler, L. J. Microstructures and electrical conductivity of nanocrystalline ceria-based thin films. *Solid State Ionics* **177**, 2513-2518 (2006).

32 Khafizov, M. *et al.* Thermal Conductivity in Nanocrystalline Ceria Thin Films. *Journal of the American Ceramic Society* **97**, 562-569 (2014).

33 SRH, D. & MD, S. Measurement of the thermal conductivity of polyacrylamide tissue-equivalent material. *International Journal of Hyperthermia* **19**, 551-562 (2003).

34 Huang, G., Zhang, Y., Ouyang, J., Baeyens, W. R. & Delanghe, J. R. Application of carbon nanotube-matrix assistant native polyacrylamide gel electrophoresis to the separation of apolipoprotein AI and complement C3. *Analytica Chimica Acta* **557**, 137-145 (2006).

35 Guo, Y. *et al.* Novel application of carbon nanotubes for improving resolution in detecting human serum proteins with native polyacrylamide gel electrophoresis. *Nano Letters* **9**, 1320-1324 (2009).

36 Pop, E., Mann, D., Wang, Q., Goodson, K. & Dai, H. Thermal conductance of an individual single-wall carbon nanotube above room temperature. *Nano Letters* **6**, 96-100 (2006).

37 Li, Q. *et al.* Structure-dependent electrical properties of carbon nanotube fibers. *Advanced Materials* **19**, 3358-3363 (2007).

38 Goharshadi, E., Ahmadzadeh, H., Samiee, S. & Hadadian, M. Nanofluids for Heat Transfer Enhancement-A Review. *Phys. Chem. Res* **1**, 1-33 (2009).

39 Kochetov, R. *et al.* Modelling of the thermal conductivity in polymer nanocomposites and the impact of the interface between filler and matrix. *Journal of Physics D: Applied Physics* **44**, 395401 (2011).
40 Kuhn, R. & Hoffstetter-Kuhn, S. *Capillary Electrophoresis: Principles and Practice.* (springer-verlag Berlin, 1993).
41 Giddings, J. C. Unified Separation Science. New York, Wiley, (1991).
42 Ito, Y. & Cazes, J. *Encyclopedia of Chromatography.* 146 (Taylor & Francis, 2001).
43 Reijenga, J. C. in *Encyclopedia of Chromatography, Second Edition* 121-121 (Taylor & Francis, 2005).
44 Goren, K., Chen, L., Schadler, L. S. & Ozisik, R. Influence of nanoparticle surface chemistry and size on supercritical carbon dioxide processed nanocomposite foam morphology. *The Journal of Supercritical Fluids* **51**, 420-427 (2010).
45 Goren, K, et al. Supercritical carbon dioxide assisted dispersion and distribution of silica nanoparticles in polymers. *The Journal of Supercritical Fluids* **67**, 108-113 (2012).